INTERNATIONAL JOURNAL OF COMPUTERS COMMUNICATIONS & CONTROL
Online ISSN 1841-9844, ISSN-L 1841-9836, Volume: 21, Issue: 4, Month: August, Year: 2026
Article Number: 7460, https://doi.org/10.15837/ijccc.2026.4.7460

Real-Time Hardware-in-the-Loop Evaluation of an RBFNN Controller for Water Level Control in an Uncertain Triple-Tank System

Trung Nhan Nguyen, Thanh Quyen Ngo, Thanh Hai Tran, Ngoc Hoi Le, Van Sy Nguyen, Tong Tan Hoa Le

Trung Nhan Nguyen*
Robotics, Intelligent control and Computer vision research group, Faculty of Electrical Engineering Technology, Industrial University of Ho Chi Minh City, Vietnam
nguyentrungnhan@iuh.edu.vn
*Corresponding author

Thanh Quyen Ngo
Robotics, Intelligent control and Computer vision research group, Faculty of Electrical Engineering Technology, Industrial University of Ho Chi Minh City, Vietnam
ngothanhquyen@iuh.edu.vn

Thanh Hai Tran
Robotics, Intelligent control and Computer vision research group, Faculty of Electrical Engineering Technology, Industrial University of Ho Chi Minh City, Vietnam
tranthanhhai@iuh.edu.vn

Ngoc Hoi Le
Faculty of Electrical Engineering Technology, Industrial University of Ho Chi Minh City, Vietnam
lengochhoi@iuh.edu.vn

Van Sy Nguyen
Faculty of Automotive Engineering Technology, Industrial University of Ho Chi Minh City, Vietnam
nguyenvansy@iuh.edu.vn

Tong Tan Hoa Le
Faculty of Electrical Engineering Technology, Industrial University of Ho Chi Minh City, Vietnam
letongtanhoa@iuh.edu.vn

Abstract

This paper addresses the problem of water-level regulation in a triple-tank system, where strong nonlinearities, dynamic coupling, external disturbances, and parameter uncertainties pose significant challenges for conventional model-based control methods. To overcome these limitations, a Radial Basis Function Neural Network (RBFNN)–based control strategy is proposed for regulating the water level in Tank 3 without requiring an accurate mathematical model of the system. The main contribution of this work lies in the real-time hardware-in-the-loop (HIL) implementation of an adaptive RBFNN-based control strategy using the OPAL-RT OP5707XG platform, enabling practical validation under realistic operating conditions. The proposed controller exploits the strong nonlinear approximation capability and fast learning characteristics of RBFNNs to enhance tracking accuracy, transient performance, and robustness under varying operating conditions. The effectiveness of the proposed method is evaluated through MATLAB/Simulink simulations and real-time HIL experiments. Two representative experimental scenarios are considered, including constant

and continuously varying water level references, to comprehensively assess steady-state accuracy, transient response, adaptability, and real-time performance. Performance is quantitatively evaluated using standard error-based indices such as RMS, MAE, Mean Error, IAE, and ISE. Both simulation and real-time experimental results demonstrate that the proposed RBFNN controller enables the water level in Tank 3 to accurately track the desired reference trajectories with reduced overshoot, faster settling time, smoother responses, and lower cumulative tracking error compared with conventional PID and sliding mode control (SMC).

Keywords: Triple-Tank System, Opal-RT, HIL, RBFNN, intelligent control.

1 Introduction

Nonlinear systems are those in which a first-order linear model cannot fully describe the input-output relationship. Due to their nonlinearity, mathematical analysis is often complex; constructing general solutions is challenging, and the synthesis and design of control systems are significantly more difficult than for linear problems [1–3]. In practice, nonlinear systems are standard in industry, especially in processes with state-varying dynamics and are strongly affected by disturbances, saturation, hysteresis, and parameter uncertainty [4–8].

In typical process applications, tank systems, such as cylindrical tanks, conical-bottom cylindrical tanks, etc., are widely used across many technological lines. Classic problems arising in process industries include chemical mixing, liquid level control, and flow control [9–13]. In addition, spherical tanks are of interest in some applications due to their favourable structural and operational characteristics. Compared to cylindrical tanks, spherical tanks generally have higher mechanical strength. They can achieve a smaller surface area-to-volume ratio, thereby reducing heat exchange with the environment and limiting operational losses. In addition, spherical tanks can provide benefits in effective cleaning, reduced maintenance costs, and improved fabrication under certain technological conditions [14–16]. These advantages make spherical tanks a worthwhile choice for storage systems and processes that require tight product quality control [17,18].

In terms of control, liquid level control is a typical problem in process control. It is widely applied in water filtration, chemical and biochemical technology, automatic liquid dispensing, food and beverage processing, and the pharmaceutical industry. Control quality directly affects product quality and equipment safety. However, real-world tank systems often exhibit unfavourable characteristics, such as strong nonlinearity, large hysteresis, complex dynamic linkages, and parameter uncertainty, making control accuracy highly dependent on the operating state, system parameters, and the control algorithm. Therefore, achieving high-precision control with linear methods alone is often not guaranteed, especially when good monitoring and noise immunity across the entire operating range are required. Consequently, to achieve high control accuracy and good tracking performance under conditions of nonlinearity and uncertainty, nonlinear control methods should be prioritised to address these issues and improve control quality.

Nowadays, many tank configurations have been studied with different approaches. Works have proposed and evaluated many strategies, such as: partially supervised reinforcement learning algorithm [19], quadratic sliding mode control combined with parameter estimation [20], PI sliding mode control integrated with backstep method [21], feedback linearization based on disturbance observer [22] and distributed model predictive control [23]. With three tanks and two inputs, a real-time optimal neural controller has been studied to improve control quality under nonlinear and uncertain conditions [24]. Meanwhile, with three tanks and one input, the adaptive predictive control approach, based on data rather than a model (combining discrete lazy learning), has been applied to increase flexibility and reduce dependence on the exact model [25]. For two-tank coupled two-input systems, solutions such as VRFT-based controllers incorporating modelless Q-learning [26] and quadratic sliding mode control [27] have also been proposed. For two-tank single-input control systems, methods such as sliding mode control and adaptive backstepping have been reported to improve tracking performance and noise immunity [28,29]. Among the above approaches, sliding mode control is often used as a robust solution to compensate for uncertainties in the system's dynamics and/or kinematics [30–35]. The outstanding advantage of sliding mode control is its robustness against noise and parameter variations; however, a common disadvantage is chattering caused by the switching control signal,

which can increase actuator wear and degrade control quality if not properly handled. In parallel, neural network-based and evolutionary optimisation methods are also practical tools for nonlinear control design. Neural network-based controllers offer advantages in adaptive learning, generalisation, and fault tolerance, but often require complex training algorithms and high computational costs [36–40]. Optimisation methods, such as genetic algorithms, are also used to find optimal control parameters/laws in nonlinear, multi-extremal environments. However, they may also have limitations in convergence time and computational resources [41–44]. Notably, many studies and experiments have shown that adaptive fuzzy control is suitable for systems with poorly defined or difficult-to-build dynamic models, and has proven to be a powerful approach to controlling nonlinear systems in many industrial contexts [45–47].

This study proposes an uncertainty approximation framework based on a Radial Basis Function Neural Network (RBFNN). RBFNNs are well known for their capability to approximate unmodeled nonlinear dynamics and uncertainties in complex systems [48]. In addition, their online learning capability enables continuous parameter adaptation, thereby improving approximation accuracy under varying operating conditions [48]–[56].

However, despite these advantages, many existing approaches either depend on accurate system modeling or lack real-time validation under practical conditions. In particular, the integration of adaptive neural approximation with hardware-in-the-loop (HIL) implementation for uncertain multi-tank systems remains relatively underexplored. Furthermore, few studies provide a comprehensive experimental comparison with classical controllers under both constant and time-varying operating scenarios.

The main contributions of this paper can be summarized as follows:

- A real-time implementation of an adaptive RBFNN-based control framework on the OPAL-RT OP5707XG HIL platform for an uncertain triple-tank system, bridging the gap between simulation-based design and practical deployment.
- Development of an adaptive RBFNN-based uncertainty estimator that operates online to approximate unknown nonlinear dynamics and external disturbances, without requiring an accurate system model.
- Experimental validation under both constant and time-varying reference signals, providing a more comprehensive assessment of tracking performance, robustness, and adaptability compared to existing studies.
- A systematic performance comparison with conventional PID and sliding mode control (SMC) using multiple quantitative error metrics, highlighting the advantages of the proposed approach in real-time operation.

The remainder of this paper is organised as follows. Section 2 presents the mathematical model of the triple-tank water system. Section 3 describes the design of the proposed control strategy. Section 4 presents the experimental results from the hardware-in-the-loop (HIL) platform and discusses the performance of the proposed method across different operating scenarios. Finally, Section 5 concludes the paper and outlines directions for future research.

2 Mathematical equation of the object

2.1 Determine the surface area and volume of the object

In many engineering applications, tank designs often feature a cylindrical body with hemispherical ends. To accurately model the storage volume with a clear mathematical basis, proving the volume formula using integration is crucial to ensuring the correctness of the design, capacity calculations, and simulation verification.

The tank is partitioned into three non-overlapping subregions consisting of the left semicircle (Partition A), the central rectangular region (Partition B), and the right semicircle (Partition C).

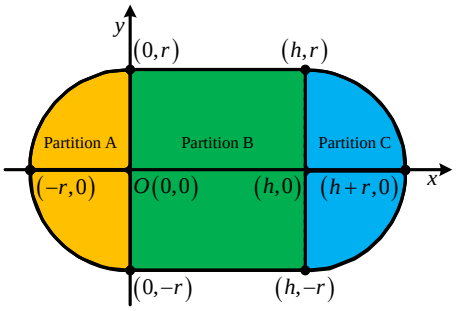

Figure 1: Cross-sectional view of the storage tank

Partition A corresponds to the left half of a circle centered at $O\,(0,0)$ with radius r, described by the equation $x^2+y^2=r^2$ over the domain $-r\le x\le 0$. The upper and lower boundaries of this region are given by $y=\sqrt{r^2-x^2}$ and $y=-\sqrt{r^2-x^2}$. The area of Partition A is determined as follows:

$$\begin{aligned} S_A &= \int_{-r}^{0}\left[\sqrt{r^2-x^2}-\left(-\sqrt{r^2-x^2}\right)\right]dx = \int_{-r}^{0} 2\sqrt{r^2-x^2}dx = 2\left[\frac{x}{2}\sqrt{r^2-x^2}+\frac{r^2}{2}\arcsin\left(\frac{x}{r}\right)\right]\Bigg|_{-r}^{0} \\ &= \left[x\sqrt{r^2-x^2}+r^2\arcsin\left(\frac{x}{r}\right)\right]\Bigg|_{-r}^{0} = 0-\left(-\frac{\pi r^2}{2}\right) = \frac{\pi r^2}{2} \end{aligned} \tag{1}$$

The volume of Partition A is determined as follows:

$$\begin{aligned} V_A &= \pi\int_{-r}^{0}(r^2-x^2)dx = \pi\left(\int_{-r}^{0} r^2dx-\int_{-r}^{0}x^2dx\right) = \pi\left(r^2\,x|_{-r}^{0}-\frac{x^3}{3}\Bigg|_{-r}^{0}\right) \\ &= \pi\left\{r^2(0-(-r))-\left[0-\left(\frac{(-r)^3}{3}\right)\right]\right\} = \pi\left(r^3-\frac{r^3}{3}\right) = \frac{2}{3}\pi r^3 \end{aligned} \tag{2}$$

Consider Partition B over the interval $0\le x\le h$, where the upper and lower boundaries are given by $y=r$ and $y=-r$, respectively. Consequently, the area of Partition B is computed by evaluating the integral with respect to the $x-axis$ as follows:

$$S_B=\int_0^h[r-(-r)]dx=\int_0^h 2rdx=2rh \tag{3}$$

A Cartesian coordinate system Oxy is established for Partition B such that the Ox axis coincides with the longitudinal axis of the cylinder and serves as the axis of rotation. When considering a cross-section taken along this axis, the upper boundary of the shape represents the radius of the cylinder at each position x. Upon rotating this region about the Ox axis, each slice perpendicular to Ox at position x forms a circular disk with radius r. Accordingly, the cross-sectional area at position is given by $A\,(x)=\pi r^2$, and the total volume is obtained by integrating this area along the length:

$$V_B=\int_0^h A(x)dx=\int_0^h \pi r^2dx=\pi r^2\int_0^h dx=\pi r^2\,x|_0^h=\pi r^2h \tag{4}$$

Similarly, Partition C corresponds to the right semicircle centered at $(h,0)$ with radius r, described by the equation $(x-h)^2+y^2=r^2$ over the interval $h\le x\le h+r$. The area of Partition C is expressed as follows:

$$S_C=\int_h^{h+r}2\sqrt{r^2-(x-h)^2}dx \tag{5}$$

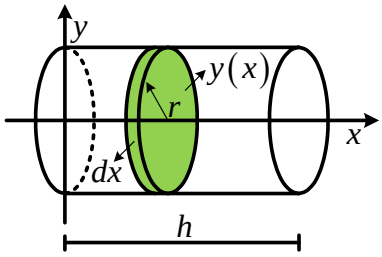

Figure 2: The method of calculating the volume of a solid of revolution by rotating it around Ox axis

Let the variable substitution $u = x - h \Rightarrow du = dx$. When $x = h \Rightarrow u = 0$ and when $x = h + r \Rightarrow u = r$. Consequently, Eq. (5) can be rewritten as:

$$S_C = \int_0^r 2\sqrt{r^2 - u^2}du = \frac{\pi r^2}{2} \tag{6}$$

The volume of the right hemispherical section in Partition C is determined as follows:

$$\begin{aligned} V_C &= \pi \int_h^{h+r} \left[r^2 - (x-h)^2\right]dx = \pi \int_0^r (r^2 - u^2)du = \pi \left(\int_0^r r^2 du - \int_0^r u^2 du\right) \\ &= \pi \left(r^2\, u|_0^r - \frac{u^3}{3}\Big|_0^r\right) = \pi \left(r^3 - \frac{r^3}{3}\right) = \frac{2}{3}\pi r^3 \end{aligned} \tag{7}$$

The area of the storage tank is determined as follows:

$$S = \frac{\pi r^2}{2} + 2rh + \frac{\pi r^2}{2} = 2rh + \pi r^2 \tag{8}$$

The total volume of the tank is the sum of three parts:

$$V = \frac{2}{3}\pi r^3 + \pi r^2 L + \frac{2}{3}\pi r^3 = \pi r^2 h + \frac{4}{3}\pi r^3 \tag{9}$$

2.2 Equation of motion of the object

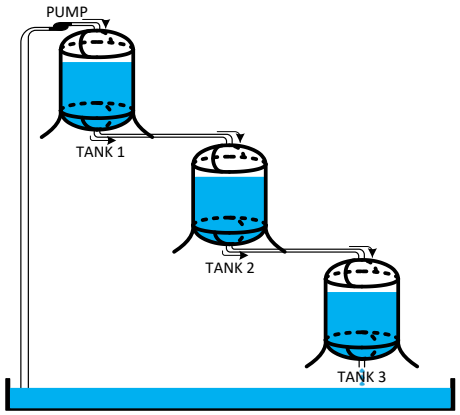

Figure 3: Schematic of Triple Tank System

The objective of this section is to formulate the dynamic equations governing the water levels in the tanks, in which the water level of each downstream tank depends on the dynamics of the preceding tank. The motion equation for L_1 is established to describe the relationship between the pump control voltage and the water level in Tank 1.

Considering the triple-tank cascaded system illustrated in Fig. 1, water is pumped into Tank 1, after which the flow from Tank 1 feeds Tank 2, and subsequently flows from Tank 2 into Tank 3. Accordingly, the dynamics of Tank 1 characterize the relationship between the input signal and

Table 1: Convention of symbols

Symbol	Meaning of the parameters	Unit
L_1	Water level in Tank 1	m
L_2	Water level in Tank 2	m
L_3	Water level in Tank 3	m
V_p	Pump input voltage	V
K_p	Proportional constant between pump voltage and inflow rate to Tank 1	$m^3/(s \cdot V)$
S_1	Cross-sectional area of Tank 1	m^2
S_2	Cross-sectional area of Tank 2	m^2
S_3	Cross-sectional area of Tank 3	m^2
F_{i1}	Inflow rate to Tank 1	m^3/s
F_{o1}	Outflow rate from Tank 1	m^3/s
F_{i2}	Inflow rate to Tank 2 (equal to outflow from Tank 1)	m^3/s
F_{o2}	Outflow rate from Tank 2	m^3/s
F_{i3}	Inflow rate to Tank 3 (equal to outflow from Tank 2)	m^3/s
F_{o3}	Outflow rate from Tank 3	m^3/s
A_{o1}	Outlet orifice area of Tank 1	m^2
A_{o2}	Outlet orifice area of Tank 2	m^2
A_{o3}	Outlet orifice area of Tank 3	m^2
g	Gravitational acceleration	m/s^2

L_1, whereas the dynamics of Tank 2 and Tank 3 describe the relationships $L_1 \rightarrow L_2$ and $L_2 \rightarrow L_3$, respectively. In this system, L_1 regulates the inflow to Tank 2, L_2 controls the inflow to Tank 3, and the final output of the system is the water level L_3. The symbols in this study are defined in Table 1.

2.2.1 Nonlinear equation of motion for the water level in tank 1

The motion equation for Tank 1 describes the relationship between the voltage applied to the pump and the water level in Tank 1. Therefore, the resulting dynamic equation can be expressed in the following form:

$$\frac{\partial L_1}{\partial t} = f\left(L_1, U_p\right) \tag{10}$$

Here, f denotes a function, L_1 represents the water level in Tank 1, and V_p is the voltage applied to the pump. By applying the principle of mass balance to Tank 1, the dynamic equation governing the water level can be derived as follows:

$$S_1 \frac{\partial L_1}{\partial t} = F_{i1} - F_{o1} \tag{11}$$

Here, S_1 denotes the cross-sectional area of Tank 1, while F_{i1} and F_{o1} represent the inflow and outflow rates of Tank 1, respectively. The volumetric inflow rate into Tank 1 is assumed to be proportional to the voltage applied to the pump:

$$F_{i1} = K_p V_p \tag{12}$$

where K_p is the pump gain. By applying Bernoulli's equation for a small orifice, the outflow velocity from Tank 1, denoted as v_{o1}, can be expressed as follows:

$$v_{o1} = \sqrt{2gL_1} \tag{13}$$

Based on Eq. (4), the outflow from Tank 1 can be expressed as follows:

$$F_{o1} = A_{o1}\sqrt{2gL_1} \tag{14}$$

The water level in Tank 1 is defined as follows:

$$S_1 \frac{\partial L_1}{\partial t} = K_p V_p - A_{o1}\sqrt{2gL_1} \tag{15}$$

Designing and implementing a linear water-level controller for the Tank 1 system first requires the development of a linearized differential model of the system. Since the original dynamic model of Tank 1 is nonlinear, linearization is performed around a nominal operating point. By definition, a steady-state equilibrium at the nominal operating point (V_{p0}, L_{10}) is achieved when the water level in Tank 1 is maintained constant at L_{10}. Under this condition, the steady inflow generated by the constant pump voltage V_{p0} ensures that the system exhibits no time variation. However, in practical water-level control of Tank 1, small deviations in the water level L_{11} and small variations in the control voltage V_{p1} exist relative to the nominal operating point (V_{p0}, L_{10}). Therefore, the variables L_1 and V_p can be expressed as the sum of their nominal values and small perturbations, as follows:

$$L_1 = L_{10} + L_{11}; V_p = V_{p0} + V_{p1} \tag{16}$$

Therefore, based on Eq. (15), the equation can be rewritten as follows:

$$\frac{\partial L_{11}}{\partial t} = f\left(L_{11}, V_{p1}\right) = \frac{K_p}{S_1}\left(V_{p0} + V_{p1}\right) - \frac{A_{o1}}{S_1}\sqrt{2g\left(L_{10} + L_{11}\right)} \tag{17}$$

where $K_1 = \left.\frac{\partial\left(\frac{K_p}{S_1}V_p - \frac{A_{o1}}{S_1}\sqrt{2gL_1}\right)}{\partial V_p}\right|_{L_1=L_{10}, V_p=V_{p0}} = \frac{K_p}{S_1}; K_2 = \left.\frac{\partial\left(\frac{K_p}{S_1}V_p - \frac{A_{o1}}{S_1}\sqrt{2gL_1}\right)}{\partial L_1}\right|_{L_1=L_{10}, V_p=V_{p0}} = -\frac{A_{o1}}{S_1}\left.\frac{\partial(2gL_1)^{\frac{1}{2}}}{\partial L_1}\right|_{L_1=L_{10}} = -\frac{A_{o1}}{S_1}\left.\left[\frac{1}{2}2g(2gL_1)^{-\frac{1}{2}}\right]\right|_{L_1=L_{10}} = -\frac{A_{o1}}{S_1}\left.\frac{g}{\sqrt{2gL_1}}\right|_{L_1=L_{10}} = -\frac{A_{o1}}{S_1}\sqrt{\frac{g}{2L_{10}}}$

2.2.2 Nonlinear equation of motion for the water level in tank 2

By applying the principle of mass balance to Tank 2, the dynamic equations can be derived:

$$S_2 \frac{\partial L_2}{\partial t} = F_{i2} - F_{o2} \tag{18}$$

Here, S_2 denotes the cross-sectional area of Tank 2, while F_{i2} and F_{o2} represent the inflow and outflow rates of the tank, respectively. The volumetric inflow rate into Tank 2 is equal to the volumetric outflow rate from Tank 1:

$$F_{i2} = F_{o1} = A_{o1}\sqrt{2gL_1} \tag{19}$$

Similar to Tank 1, by applying Bernoulli's equation for small orifices, the outflow velocity from Tank 2 can be expressed as follows:

$$v_{o2} = \sqrt{2gL_2} \tag{20}$$

Based on Eq. (20), the outflow from Tank 1 can be expressed as follows:

$$F_{o2} = A_{o2}\sqrt{2gL_2} \tag{21}$$

By substituting Eq. (19) and Eq. (21) into Eq. (18), Eq. (22) is obtained:

$$S_2 \frac{\partial L_2}{\partial t} = A_{o1}\sqrt{2gL_1} - A_{o2}\sqrt{2gL_2} \tag{22}$$

Similar to Tank 1, the water-level dynamics of Tank 2 are linearized around the nominal operating point (L_{10}, L_{20}). When the system operates in the vicinity of the equilibrium point, it is assumed that the water levels L_1 and L_2 deviate only slightly, denoted by (L_{11}, L_{22}), from their nominal values. Therefore, L_1 and L_2 can be expressed as the sum of their nominal values and small perturbations, facilitating the construction of a linearized model.

$$L_2 = L_{20} + L_{22}; L_1 = L_{10} + L_{11} \tag{23}$$

Substituting Eq. (23) into Eq. (22) yields:

$$\frac{\partial L_{22}}{\partial t} = f\left(L_{11}, L_{22}\right) = \frac{A_{o1}}{S_2}\sqrt{2g\left(L_{10}+L_{11}\right)} - \frac{A_{o2}}{S_2}\sqrt{2g\left(L_{20}+L_{22}\right)} \tag{24}$$

By applying a Taylor series to Eq. (24), Eq. (25) is obtained:

$$l\frac{\partial L_{22}}{\partial t} = f\left(L_{11}, L_{22}\right) = f\left(L_{10}, L_{20}\right) + K_3 L_{11} + K_4 L_{22} \tag{25}$$

where $K_3 = \left.\frac{\partial\left(\frac{A_{o1}}{S_2}\sqrt{2gL_1} - \frac{A_{o2}}{S_2}\sqrt{2gL_2}\right)}{\partial L_1}\right|_{L_1=L_{10}, L_1=L_{20}} = \left.\frac{A_{o1}}{S_2}\frac{\partial(2gL_1)^{\frac{1}{2}}}{\partial L_1}\right|_{L_1=L_{10}} = \left.\frac{A_{o1}}{S_2}\left[\frac{1}{2}2g(2gL_1)^{-\frac{1}{2}}\right]\right|_{L_1=L_{10}} = \left.\frac{A_{o1}}{S_2}\frac{g}{\sqrt{2gL_1}}\right|_{L_1=L_{10}} = \frac{A_{o1}}{S_2}\sqrt{\frac{g}{2L_{10}}}; K_4 = \left.\frac{\partial\left(\frac{A_{o1}}{S_2}\sqrt{2gL_1} - \frac{A_{o2}}{S_2}\sqrt{2gL_2}\right)}{\partial L_2}\right|_{L_1=L_{10}, L_1=L_{20}} = -\left.\frac{A_{o2}}{S_2}\frac{\partial(2gL_2)^{\frac{1}{2}}}{\partial L_2}\right|_{L_2=L_{20}} = -\left.\frac{A_{o2}}{S_2}\left[\frac{1}{2}2g(2gL_2)^{-\frac{1}{2}}\right]\right|_{L_2=L_{20}} = -\left.\frac{A_{o2}}{S_2}\frac{g}{\sqrt{2gL_2}}\right|_{L_2=L_{20}} = -\frac{A_{o2}}{S_2}\sqrt{\frac{g}{2L_{20}}}$.

2.2.3 Nonlinear equation of motion for the water level in tank 3

By applying the principle of mass balance to Tank 3, the dynamic equation can be derived:

$$S_3\frac{\partial L_3}{\partial t} = F_{i3} - F_{o3} \tag{26}$$

Here, S_3 denotes the cross-sectional area of Tank 3, while F_{i3} and F_{o3} represent the inflow and outflow rates of the tank, respectively. The volumetric inflow rate into Tank 3 is equal to the volumetric outflow rate from Tank 2:

$$F_{i3} = F_{o2} = A_{o2}\sqrt{2gL_2} \tag{27}$$

Similar to Tank 2, by applying Bernoulli's equation for small orifices, the outflow velocity from Tank 3 can be expressed as follows:

$$v_{o3} = \sqrt{2gL_3} \tag{28}$$

The outflow from Tank 3 can be expressed as follows:

$$F_{o3} = A_{o3}\sqrt{2gL_3} \tag{29}$$

Eq. (30) results from substituting (27) and (29) into (26):

$$S_3\frac{\partial L_3}{\partial t} = A_{o2}\sqrt{2gL_2} - A_{o3}\sqrt{2gL_3} \tag{30}$$

Similar to Tank 2, the water-level dynamics of Tank 3 are linearized around the nominal operating point (L_{20}, L_{30}). When the system operates near the equilibrium point, it is assumed that the water levels L_2 and L_3 deviate only slightly, denoted by (L_{22}, L_{33}), from their nominal values. Therefore, L_2 and L_3 can be expressed as the sum of their nominal values and small perturbations, which facilitates the development of a linearized model.

$$L_3 = L_{30} + L_{33}; L_2 = L_{20} + L_{22} \tag{31}$$

Substituting Eq. (31) into Eq. (30) yields:

$$\frac{\partial L_{33}}{\partial t} = f\left(L_{22}, L_{33}\right) = \frac{A_{o2}}{S_3}\sqrt{2g\left(L_{20}+L_{22}\right)} - \frac{A_{o3}}{S_3}\sqrt{2g\left(L_{30}+L_{33}\right)} \tag{32}$$

By applying a Taylor series approximation to Eq. (32), Eq. (33) is obtained:

$$\frac{\partial L_{33}}{\partial t} = f\left(L_{22}, L_{33}\right) = f\left(L_{20}, L_{30}\right) + K_5 L_{22} + K_6 L_{33} \tag{33}$$

where $K_5 = \left.\frac{\partial\left(\frac{A_{o2}}{S_3}\sqrt{2gL_2}-\frac{A_{o3}}{S_3}\sqrt{2gL_3}\right)}{\partial L_2}\right|_{L_2=L_{20},L_3=L_{30}} = \left.\frac{A_{o2}}{S_3}\frac{\partial(2gL_2)^{\frac{1}{2}}}{\partial L_2}\right|_{L_2=L_{20}} = \left.\frac{A_{o2}}{S_3}\left[\frac{1}{2}2g(2gL_2)^{-\frac{1}{2}}\right]\right|_{L_2=L_{20}} = \left.\frac{A_{o2}}{S_3}\frac{g}{\sqrt{2gL_2}}\right|_{L_2=L_{20}} = \frac{A_{o2}}{S_3}\sqrt{\frac{g}{2L_{20}}}; K_6 = \left.\frac{\partial\left(\frac{A_{o2}}{S_3}\sqrt{2gL_2}-\frac{A_{o3}}{S_3}\sqrt{2gL_3}\right)}{\partial L_3}\right|_{L_2=L_{20},L_3=L_{30}} = -\left.\frac{A_{o3}}{S_3}\frac{\partial(2gL_3)^{\frac{1}{2}}}{\partial L_3}\right|_{L_3=L_{30}} = -\left.\frac{A_{o3}}{S_3}\left[\frac{1}{2}2g(2gL_3)^{-\frac{1}{2}}\right]\right|_{L_3=L_{30}} = -\left.\frac{A_{o3}}{S_3}\frac{g}{\sqrt{2gL_3}}\right|_{L_3=L_{30}} = -\frac{A_{o3}}{S_3}\sqrt{\frac{g}{2L_{30}}}$

Differentiating Eq. (33) and neglecting the constant equilibrium term yields:

$$\ddot{L}_{33} = K_5\dot{L}_{22} + K_6\dot{L}_{33} \tag{34}$$

Substituting Eq. (25) into Eq. (34) and neglecting the constant equilibrium term yields:

$$\ddot{L}_{33} = K_5(K_3L_{11} + K_4L_{22}) + K_6\dot{L}_{33} = K_5K_3L_{11} + K_5K_4L_{22} + K_6\dot{L}_{33} \tag{35}$$

Rearranging the right-hand side of Eq. (35) and substituting it into the left-hand side of Eq. (35):

$$\begin{aligned}\ddot{L}_{33} &= K_5K_3L_{11} + K_5K_4\left(\frac{\dot{L}_{33} - K_6L_{33}}{K_5}\right) + K_6\dot{L}_{33} = K_5K_3L_{11} + K_4\left(\dot{L}_{33} - K_6L_{33}\right) + K_6\dot{L}_{33} \\ &= K_5K_3L_{11} + K_4\dot{L}_{33} - K_4K_6L_{33} + K_6\dot{L}_{33} = K_5K_3L_{11} - K_4K_6L_{33} + \dot{L}_{33}\left(K_4 + K_6\right)\end{aligned} \tag{36}$$

Let $A = -\left(K_4 + K_6\right); B = K_5K_3; C = -K_4K_6$. Eq. (36) can then be rewritten as follows:

$$\ddot{L}_{33} = A\dot{L}_{33} + BL_{11} + CL_{33} \tag{37}$$

However, in practice, there exist uncertainty components. Accordingly, Eq. (30) can be rewritten:

$$\ddot{L}_{33} = A_0\dot{L}_{33} + B_0L_{11} + C_0L_{33} + \Delta A_0\dot{L}_{33} + \Delta B_0L_{11} + \Delta C_0L_{33} = A_0\dot{L}_{33} + B_0L_{11} + C_0L_{33} + d \tag{38}$$

where $d = \Delta A_0\dot{L}_{33} + \Delta B_0L_{11} + \Delta C_0L_{33}$ represents the nonlinear uncertain terms, which are bounded by a positive constant I_{CC} as follows:

$$I \le I_{CC} \tag{39}$$

The controller is designed to ensure that L_{33} tracks L_{d33} as closely as possible. Accordingly, the tracking error is defined as follows:

$$e = L_{d33} - L_{33} \tag{40}$$

The sliding surface is defined as follows:

$$s = ke + \dot{e} \tag{41}$$

The ideal controller is designed as follows:

$$u_{ideal} = \frac{1}{B_0}(\ddot{L}_{d33} - A_0\dot{L}_{d33} - C_0L_{d33} - d + k\dot{e}) \tag{42}$$

However, in practical systems, uncertainty terms inevitably exist. Therefore, this study employs a radial basis function neural network (RBFNN) to estimate the uncertain term d in Eq. (42).

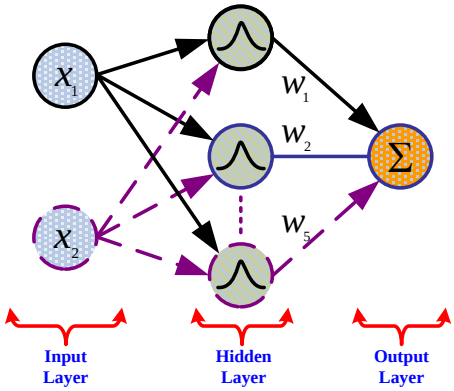

Figure 4: Structure of Radial Basis Function Neural Network

3 Controllers Design

RBFNN is a triple-layer neural network (input – hidden – output) proposed by Moody and Darken in the late 1980s. The network has good approximation capabilities for continuous functions, notable for its strong local approximation. Data is transmitted linearly from the input layer to the hidden layer, transformed non-linearly (usually using Gaussian functions), and then transmitted linearly to the output layer to produce the result as described in Fig. 4.

$$h_j = \exp\left(-\frac{\|-\mathbf{c}_j\|^2}{2b_j^2}\right), j = 1, 2, \ldots, 5 \tag{43}$$

where $\underline{\boldsymbol{x}} = [x_1, x_2, \ldots, x_n]^T$ is input layer. Each neuron uses a Gaussian activation function, $\mathbf{c}_j = [\mathrm{c}_{1j}, \mathrm{c}_{2j}]^T$ is center vector and b_j is width of the jth net of Gaussian function of RBF.

The RBF neural network is used to approximate the total disturbance d:

$$d = \mathbf{W}^{*T}\mathbf{H}\left(\underline{\boldsymbol{x}}\right) + \varepsilon \tag{44}$$

where ε is the approximate error, $\mathbf{W}^{*T} = [w_1^*, w_2^*, \ldots, w_5^*]$ is the ideal weight matrix. An online adaptive method is proposed to adjust the weight matrix $\mathbf{W}$, aiming at achieving the ideal weight matrix $\mathbf{W}^*$. Then, the output of the real-time neural network can be represented as follows:

$$\hat{d} = \hat{\mathbf{W}}^T\mathbf{H}\left(\underline{\boldsymbol{x}}\right) \tag{45}$$

where $\hat{d}$ is an approximation of the total disturbance d, and $\hat{\mathbf{W}}^T = [\hat{w}_1, \hat{w}_2, \ldots, \hat{w}_5]$ is the adaptive weight matrix. The weight adaptation law $\dot{\hat{\mathbf{W}}}^T = [\dot{\hat{w}}_1, \dot{\hat{w}}_2, \ldots, \dot{\hat{w}}_5]$ is expressed as follows:

$$\dot{\hat{\mathbf{W}}} = \delta s\mathbf{H}\left(\underline{\boldsymbol{x}}\right) \tag{46}$$

where $\delta > 0$ is gain factor. When the approximate value of the total disturbance $\hat{d}$ is inserted into Eq. (42), the control expression is obtained as follows:

$$u_{control} = \frac{1}{B_0}\left(\ddot{L}_{d33} - A_0\dot{L}_{d33} - C_0L_{d33} - \hat{d} + k\dot{e}\right) \tag{47}$$

Proof. The Lyapunov function is defined as follows:

$$\mathcal{L} = \frac{1}{2}s^2 + \frac{1}{2\eta}\tilde{\mathbf{W}}^T\tilde{\mathbf{W}} \tag{48}$$

where $\tilde{\mathbf{W}} = \mathbf{W}^* - \hat{\mathbf{W}}$. The derivative of Eq. (48) yields the following result:

$$\dot{\mathcal{L}} = s\dot{s} + \frac{1}{\eta}\tilde{\mathbf{W}}^T\dot{\tilde{\mathbf{W}}} = s\left[k\dot{e} + \left(\ddot{L}_{d33} - A_0\dot{L}_{d33} - C_0L_{d33} - B_0u - d\right)\right] - \frac{1}{\eta}\tilde{\mathbf{W}}^T\dot{\hat{\mathbf{W}}} \tag{49}$$

Substitute the derivative of Eq. (41) into Eq. (49) to obtain:

$$\begin{aligned}\dot{\mathcal{L}} &= s\left[k\dot{e} + \left(\ddot{L}_{d33} - A_0\dot{L}_{d33} - C_0L_{d33} - B_0u - d\right)\right] - \frac{1}{\eta}\tilde{\mathbf{W}}^T\dot{\tilde{\mathbf{W}}} \\ &= s\left\{k\dot{e} + k_2\left[\ddot{L}_{d33} - A_0\dot{L}_{d33} - C_0L_{d33} - \left(\ddot{L}_{d33} - A_0\dot{L}_{d33} - C_0L_{d33} - \hat{d} + k\dot{e}\right) - d\right]\right\} - \frac{1}{\eta}\tilde{\mathbf{W}}^T\dot{\tilde{\mathbf{W}}} \\ &= s\left(\hat{d} - d\right) - \frac{1}{\eta}\tilde{\mathbf{W}}^T\dot{\tilde{\mathbf{W}}}\end{aligned} \tag{50}$$

Substituting the expressions in Eq. (44) and Eq. (45) into Eq. (50), the result is as follows:

$$\begin{aligned}\dot{\mathcal{L}} &= s\left[-\hat{\mathbf{W}}^T\mathbf{H}\left(\underline{\boldsymbol{x}}\right) + \mathbf{W}^{*T}\mathbf{H}\left(\underline{\boldsymbol{x}}\right) + \varepsilon\right] - \frac{1}{\eta}\tilde{\mathbf{W}}^T\dot{\tilde{\mathbf{W}}} = s\left[\tilde{\mathbf{W}}^T\mathbf{H}\left(\underline{\boldsymbol{x}}\right) + \varepsilon\right] - \frac{1}{\eta}\tilde{\mathbf{W}}^T\dot{\tilde{\mathbf{W}}} \\ &= \tilde{\mathbf{W}}^T\left[s\mathbf{H}\left(\underline{\boldsymbol{x}}\right) - \frac{1}{\eta}\dot{\tilde{\mathbf{W}}}\right] - s\left[\varepsilon\right]\end{aligned} \tag{51}$$

Finally, applying the weight adaptation law Eq. (46) to Eq. (51) leads to the following expression:

$$\dot{\mathcal{L}} = \tilde{\mathbf{W}}^T\left[s\mathbf{H}\left(\underline{\boldsymbol{x}}\right) - s\mathbf{H}\left(\underline{\boldsymbol{x}}\right)\right] - s\varepsilon = -s\varepsilon \leq -|s|\,|\varepsilon| \leq 0 \tag{52}$$

From Eq. (52), it can be observed that $-|s|\,|\varepsilon|$. Therefore, the system achieves global asymptotic stability, with $s \to 0$ and $e \to 0$ as $t \to \infty$.

4 Results and Discussion

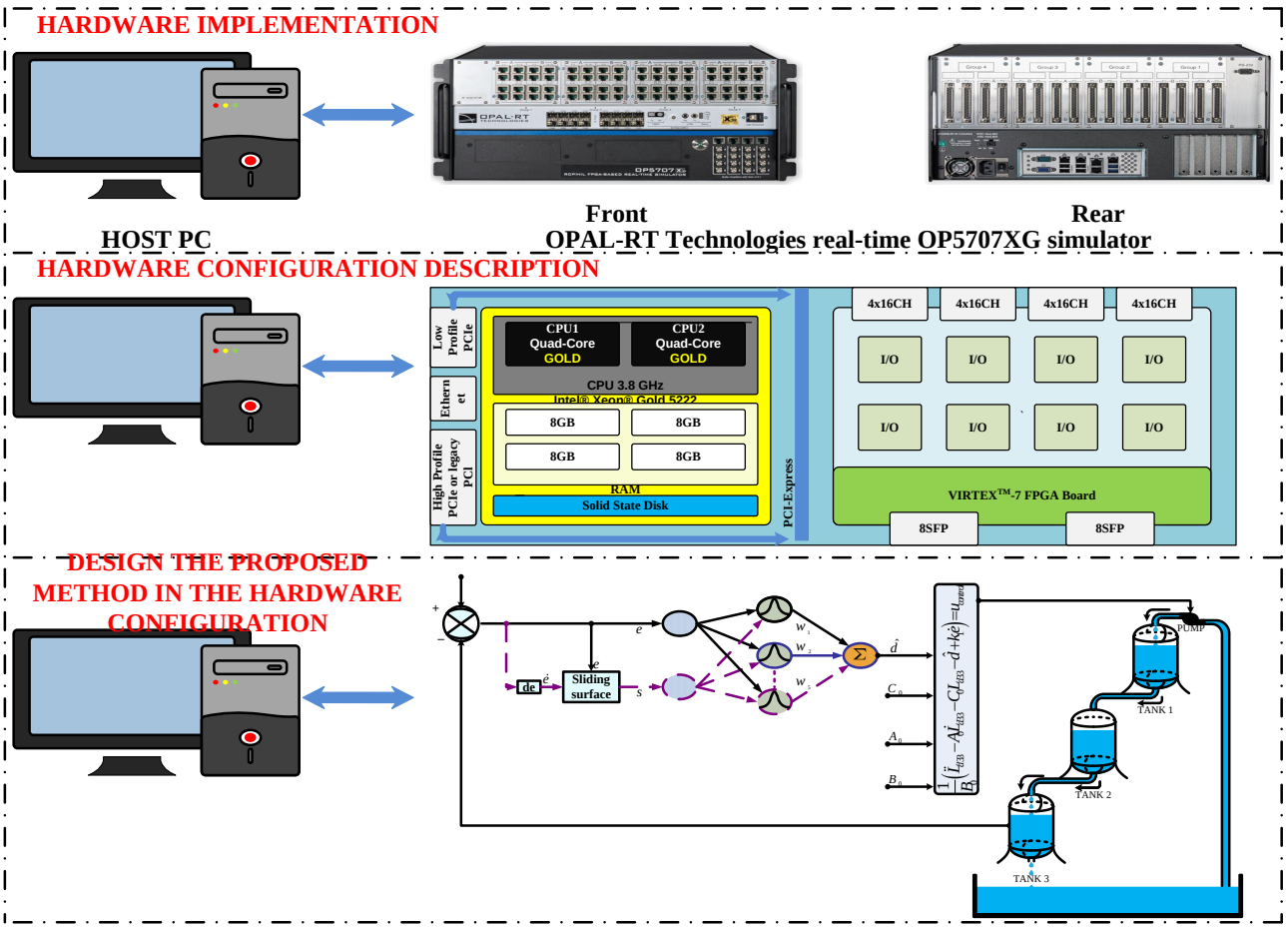

Figure 5: Real-time implementation of the proposed RBFNN-based controller for the Triple-tank water level system

Experiments were conducted on a hardware-in-the-loop (HIL) simulation platform to evaluate the feasibility, accuracy, and real-time performance of the proposed control method. The use of HIL enables verification of the control algorithm under conditions close to real-world operation while ensuring the safety and repeatability of the test scenarios. The experimental system was built using the OPAL-RT OP5707XG real-time simulator, directly connected to the host PC via Ethernetas shown in Figure 5. The simulator was equipped with a parallel-processing architecture featuring two Intel® Xeon® Gold 5222 processors, each with 4 cores and a clock speed of 3.8 GHz, along with RAM to meet the real-time computing requirements of the system model. The experiments were designed to evaluate control accuracy through criteria such as response level, settling time, and resistance to uncertainties when implemented on real-time hardware. The real-time implementation was carried out with a sampling time of Ts = 50 μs. The neural network consists of 5 radial basis neurons, with the learning rate $\eta = 0.5$ and $\delta = 0.5$. The centers of the basis functions are selected within the interval [-1, 1], and the width parameter is set to b = 1.

In this study, the performance of the PID, SMC, and RBFNN controllers is compared using error-based performance indices. Root Mean Square (RMS), Mean Absolute Error (MAE), and Mean Error (ME) are used to quantify the system's overall tracking accuracy. In addition, time-integral performance indices, including the Integral of Absolute Error (IAE) and the Integral of Squared Error (ISE), are utilised to evaluate the cumulative control effectiveness throughout the operating period. Furthermore, the settling time within the 2% and 5% tolerance bands is used to analyse the response speed and the system's ability to maintain stable operation. The combination of these performance indices enables a comprehensive, objective, and consistent comparison of the control performance among the investigated control strategies.

4.1 Maintain a stable water level at a certain value

In the first scenario, the reference water level is maintained at a fixed operating value. The objective of this experiment is to evaluate the steady-state accuracy, transient response characteristics, and disturbance rejection capability of the control strategies when implemented on the hardware-in-the-loop (HIL) platform. Key performance indices, including overshoot, settling time, and steady-state error, are monitored and analysed to assess the robustness and reliability of the controllers under uncertain operating conditions. This scenario provides a baseline for comparing the dynamic behaviour and stability properties of different control methods before considering more challenging cases with time-varying reference signals.

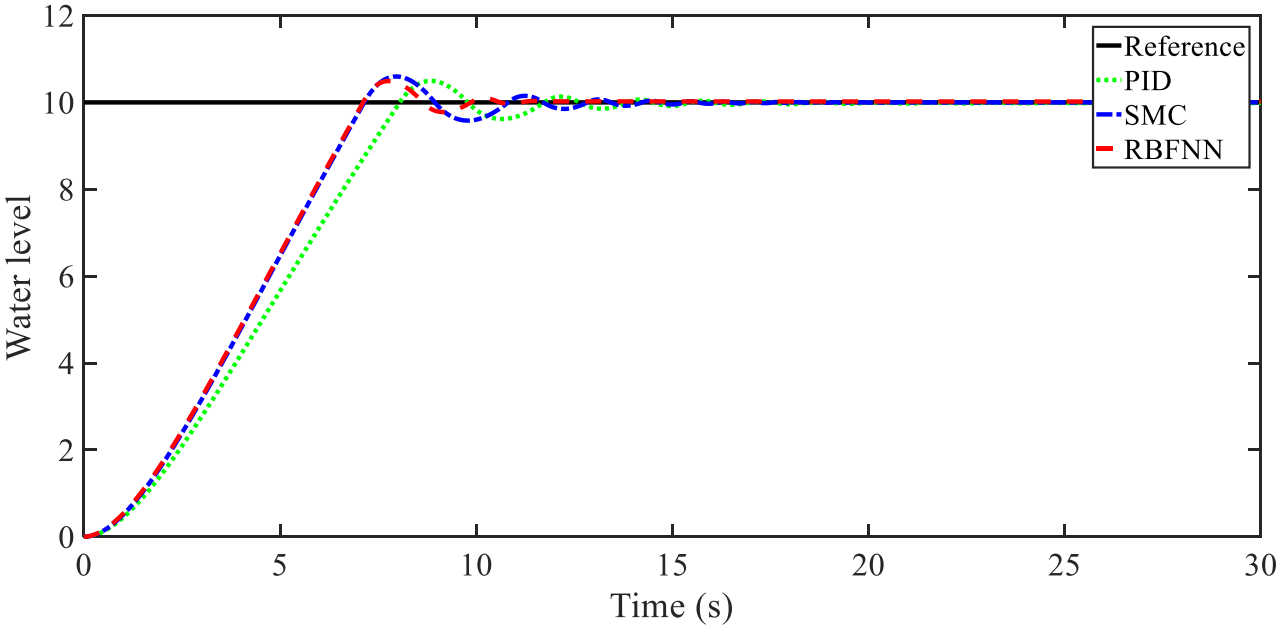

Figure 6: Water level response over time under different control methods

Figure 6 shows the water level response of the system under the influence of PID, SMC, and RBFNN controllers when tracking a reference value. It can be observed that all methods can track the setpoint signal; however, the controllers' accuracy differs significantly. The PID controller exhibits a slower response time and significant oscillations during the transient phase. Meanwhile, the SMC controller improves the response speed but still exhibits oscillations and overshoot, which can affect the actuator's lifespan when implemented in a real system. Conversely, the RBFNN controller shows a clear advantage, reaching the reference value faster, exhibiting a smaller overshoot amplitude, and showing significantly reduced oscillations. Thanks to its efficient nonlinear approximation and online adaptation, the RBFNN can compensate for system uncertainties and parameter variations better than other control methods.

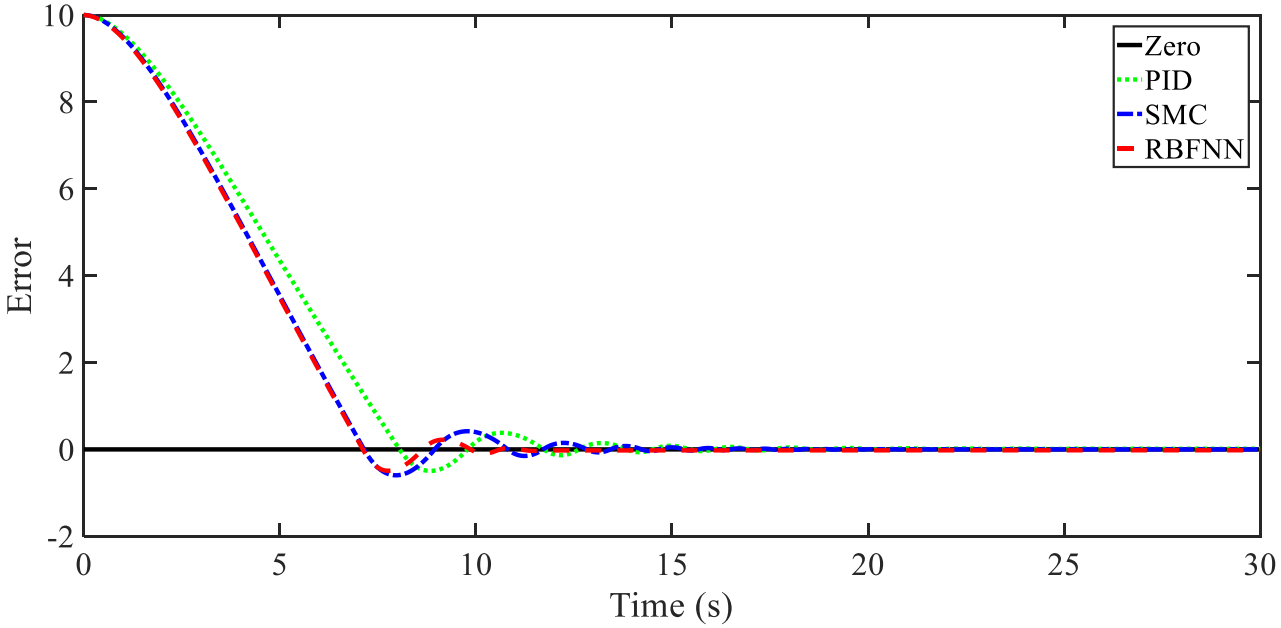

Figure 7: Tracking error under different control methods

Figure 7 shows the tracking error of the system when using PID, SMC, and RBFNN controllers. Initially, the error decreased rapidly for all methods, indicating effective control during the transient phase. However, differences in control quality became apparent during the steady-state phase. The PID controller exhibited slower error decay and small oscillations around the equilibrium point. The SMC controller significantly improved the speed of error suppression; however, residual oscillations persisted during the initial steady-state phase, which could lead to vibrations or chattering in a practical implementation. Meanwhile, the RBFNN controller showed a clear advantage, bringing the error closer to zero faster, with the smallest oscillation amplitude and the shortest settling time among the methods. Thanks to its ability to learn and approximate the nonlinear characteristics of the system, RBFNN can effectively adapt to uncertainties and disturbances, thereby minimising residual errors in both transient and steady-state phases.

Figure 8 presents a quantitative comparison of the control performance of PID, SMC, and RBFNN controllers based on several error indices, including RMS, MAE, ME, IAE, and ISE, where lower values indicate better performance. It is evident that the RBFNN controller consistently achieves the lowest values across all metrics, confirming its superior error reduction capability. In terms of RMS, the RBFNN achieves a value of 2.831, corresponding to a reduction of approximately 14.6% compared to PID (3.317) and 10.5% compared to SMC (3.163). Similarly, the MAE is reduced by about 20.0% compared to PID and 11.6% compared to SMC. The mean error (ME) also shows noticeable improvement, decreasing by approximately 21.3% and 12.0% relative to PID and SMC, respectively. For the integral performance indices, the RBFNN reduces IAE by approximately 26.0% compared to PID and 19.9% compared to SMC. A similar trend is observed in ISE, where reductions of approximately 20.3% and 26.5% are achieved compared to PID and SMC, respectively. These reductions indicate that the RBFNN not only minimizes instantaneous errors but also significantly

decreases the accumulated error over time.

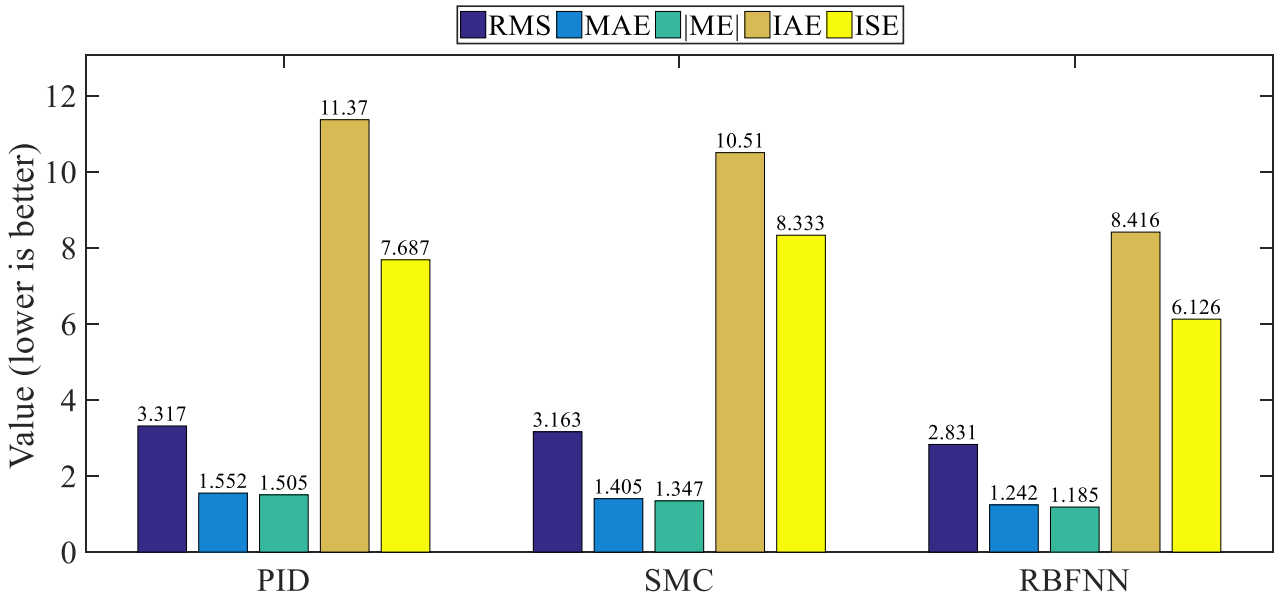

Figure 8: Quantitative performance comparison of PID, SMC, and RBFNN controllers based on error-based indices

4.2 Water-level control under time-varying reference conditions

In the second scenario, the water-level reference follows a time-varying trajectory according to a predefined time-dependent trajectory, which more closely reflects the operational requirements of practical water-level control systems. Unlike step-type reference changes, this scenario introduces dynamic variations in the setpoint, posing greater challenges to the control system in terms of tracking accuracy, adaptability, and real-time performance. The primary objective of this experiment is to evaluate the ability of the proposed control strategy to accurately track time-varying reference signals while maintaining system stability under continuously changing operating conditions. Particular attention is given to the controller's capability to adapt to rapid variations in the reference trajectory and to compensate for system nonlinearities and uncertainties during real-time implementation. Tracking performance is assessed using multiple criteria, including tracking error magnitude, the smoothness of the system response, and robustness to dynamic disturbances.

Figure 9 shows the water level response of the system when the reference signal changes continuously, reflecting the actual operating conditions of the water level control system. The PID, SMC, and RBFNN controllers can all track the reference trajectory; however, their tracking performance and response quality differ significantly, especially during rapid setpoint changes. Observation of the magnified areas (ZOOM1 and ZOOM2) shows that the PID controller exhibits tracking lag and relatively large oscillations after each change in the reference value. The SMC controller improves response speed but still exhibits residual oscillations during the transient phase, which can compromise the system's smoothness in practical applications. Conversely, the RBFNN controller demonstrates superior trajectory tracking, with low lag, low oscillation amplitude, and a smoother response to continuous changes in the reference signal. In particular, in the magnification regions, the RBFNN quickly stabilises around the new set value without causing significant oscillations, demonstrating its effective adaptability to dynamic system changes. This advantage stems from the RBFNN's online learning and nonlinear approximation capabilities, allowing the controller to better compensate for model uncertainties and noise in real-time environments.

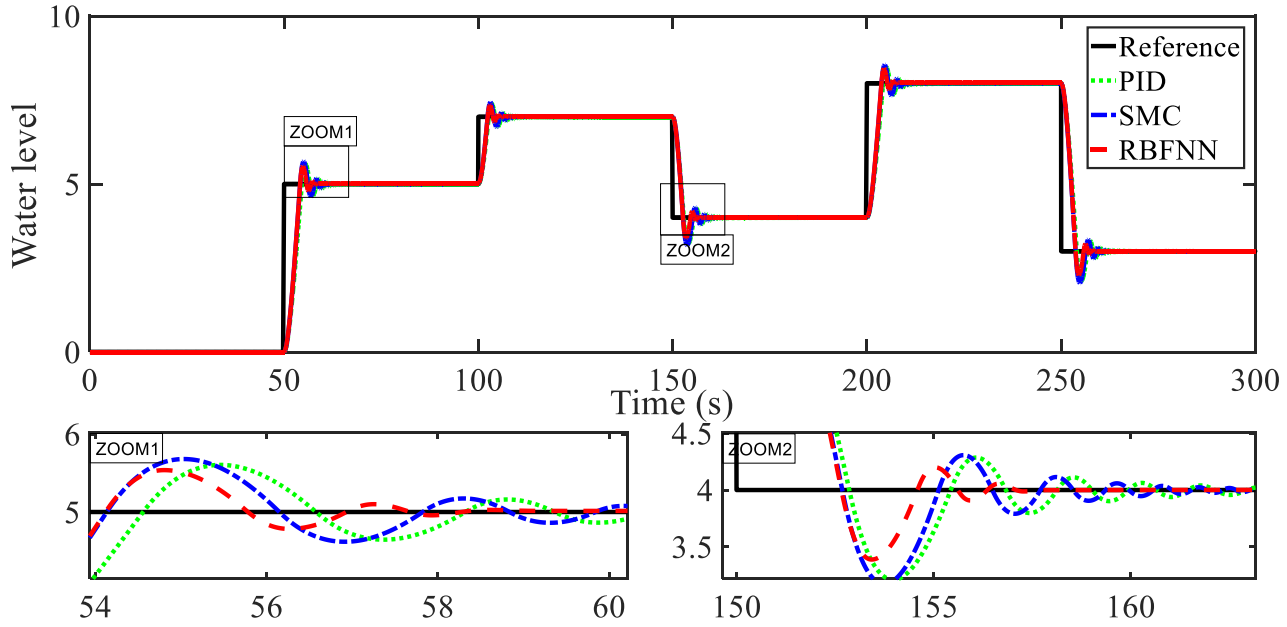

Figure 9: Water level tracking response under continuously varying reference using PID, SMC, and RBFNN controllers

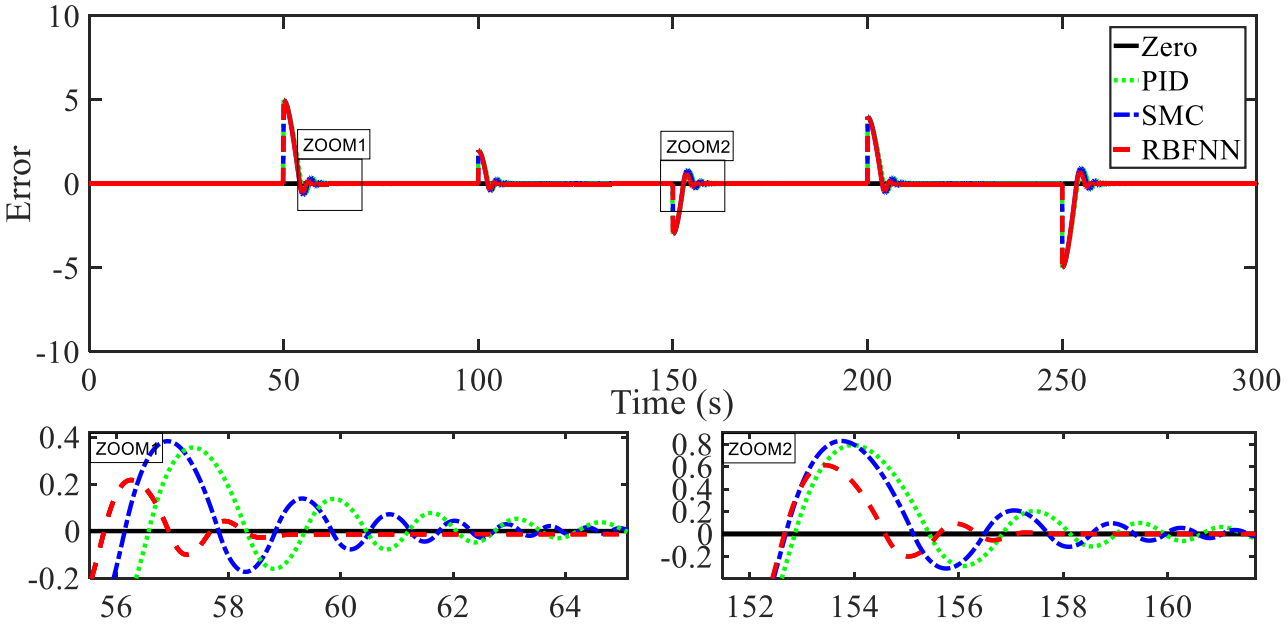

Figure 10: Water level tracking response under continuously varying reference using PID, SMC, and RBFNN controllers

Figure 10 shows the system's tracking error when the water-level reference signal changes continuously. The error mainly occurs during rapid changes in the reference trajectory, while in the remaining time intervals, the system maintains near-zero error, indicating the stable tracking capability of the compared control methods. Observation of the magnified areas (ZOOM1 and ZOOM2) shows that the PID controller exhibits a larger error amplitude and a longer error decay time, indicating limited adaptability to dynamic changes in the setpoint. The SMC controller significantly improves error suppression speed; however, residual oscillations persist during the transient phase, which can compromise response smoothness and cause vibrations in practical applications. Conversely, the RBFNN controller shows a clear advantage with faster error decay, the smallest error amplitude, and effective damping of oscillations after each change in the reference trajectory. Within the magnification

regions, the RBFNN quickly reduces the error to near zero without causing significant oscillations, demonstrating high adaptability and superior stability.

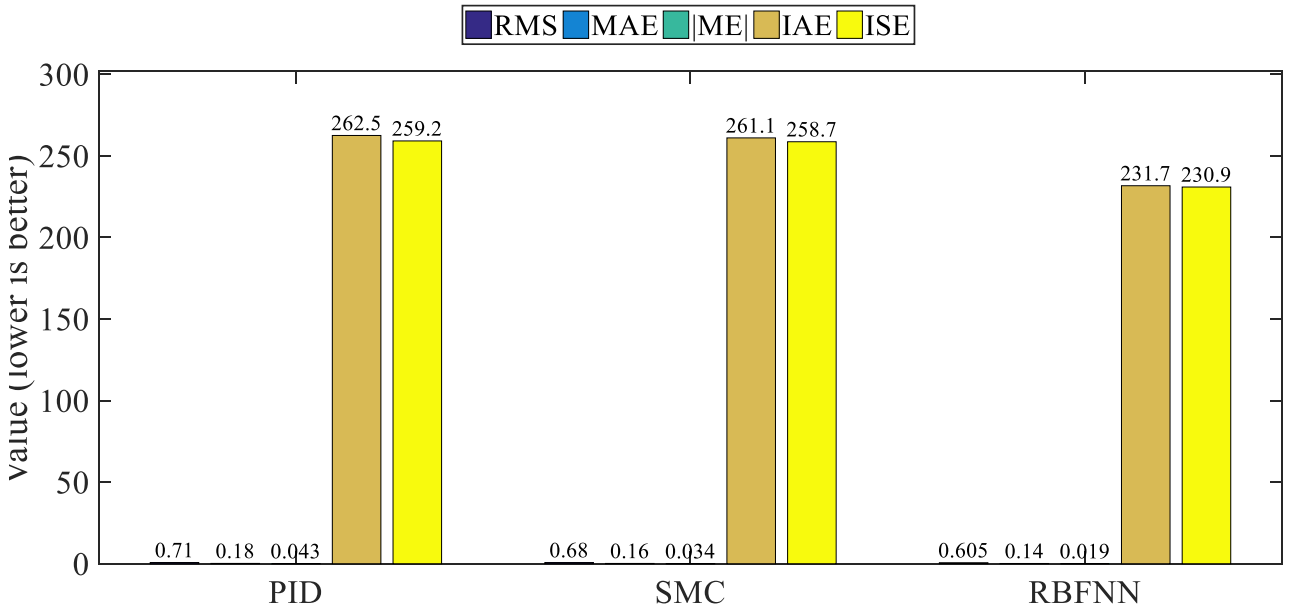

Figure 11: Comparison of RMS, MAE, Mean Error, IAE, and ISE for continuously varying reference conditions

Figure 11 presents a quantitative comparison of the control performance of PID, SMC, and RBFNN controllers under continuously varying reference conditions. The evaluation metrics include RMS, MAE, Mean Error (ME), IAE, and ISE, where lower values indicate better performance. It is evident that the RBFNN controller consistently achieves the lowest values across all criteria, confirming its superior error-reduction capability. Specifically, the RBFNN achieves an RMS value of 0.605, corresponding to a reduction of approximately 14.8% compared to PID (0.71) and 11.0% compared to SMC (0.68). Similarly, the MAE is reduced by about 22.2% relative to PID and 12.5% relative to SMC. The mean error (ME) also shows a substantial decrease, with reductions of approximately 55.8% compared to PID and 44.1% compared to SMC, indicating a significant reduction in residual bias. For the integral performance indices, the RBFNN reduces IAE by approximately 11.7% compared to PID and 11.3% compared to SMC. Likewise, the ISE is reduced by about 10.9% and 10.7%, respectively. These improvements demonstrate that the RBFNN not only minimizes instantaneous tracking errors but also effectively reduces the accumulated error over time, particularly under rapidly changing reference conditions.

In practical implementations, factors such as sensor noise, communication delays may affect control precision. Although these effects are partially reflected in the HIL environment, further investigation under real industrial conditions would be necessary to fully validate the robustness of the proposed controller.

5 Conclusion

This paper investigates the application of a Radial Basis Function Neural Network (RBFNN)–based control strategy for water-level regulation in a triple-tank system, with a particular focus on controlling the water level in Tank 3. The proposed controller is implemented and validated on a hardware-in-the-loop (HIL) platform using the OPAL-RT OP5707XG real-time simulator, enabling realistic evaluation under real-time constraints.

A key advantage of the RBFNN-based controller is that it does not require an accurate mathematical model of the highly nonlinear triple-tank system. By leveraging its strong nonlinear approximation capabilities and online learning mechanism, the RBFNN can effectively compensate for system nonlinearities, external disturbances, and parameter uncertainties in real time. Two experimental scenarios

were conducted to comprehensively assess the controller performance under different operating conditions, including constant and continuously varying reference water levels. Both simulation and HIL experimental results demonstrate that the proposed RBFNN controller enables the water level in Tank 3 to accurately track the reference trajectories with fast transient response, reduced overshoot, and smooth steady-state behaviour. Quantitative performance evaluation further confirms that RBFNN consistently achieves the lowest RMS, MAE, Mean Error, IAE, and ISE values when compared with conventional PID and sliding mode control (SMC) methods across all test scenarios. The superior performance of the RBFNN controller highlights its robustness and adaptability in handling dynamic reference changes and system uncertainties, making it particularly suitable for real-time implementation in practical water level control applications.

Despite these advantages, the performance of the RBFNN controller still depends on the selection of network parameters and learning rates, and its sensitivity to measurement noise remains uninvestigated. Future work will focus on experimental validation on a physical triple-tank system, automatic optimisation of neural network parameters, enhancement of noise robustness, and extension of the proposed approach to more complex operating conditions and disturbance scenarios.

Funding

This research received no external funding.

Author contributions

The authors contributed equally to this work.

Conflict of interest

The authors declare no conflict of interest.

References

[1] Kumar DD, Meenakshipriya B, Ram SS. Design of PSO based I-PD controller and PID controller for a spherical tank system. Indian J Sci Technol 2016;9(12):1–5.

[2] Kumar DD, Meenakshipriya B. Design and implementation of nonlinear system using gain scheduled PI controller. Procedia Eng 2012;38:3105–3112.

[3] Vincent AK, Nersisson R. Particle swarm optimization based PID controller tuning for level control of two tank system. In: Proceedings of the IOP Conference Series: Materials Science and Engineering. vol. 263. IOP Publishing; 2017. p. 052001.

[4] Prasad GM, Rao AS. Evaluation of gap-metric based multi-model control schemes for nonlinear systems: an experimental study. ISA Trans 2019;94:246–254.

[5] Rajesh P, Shajin FH, Rajani B, Sharma D. An optimal hybrid control scheme to achieve power quality enhancement in micro grid connected system. Int J Numer Model Electron Netw Devices Fields 2022:e3019.

[6] Shajin FH, Rajesh P, Thilaha S. Bald eagle search optimization algorithm for cluster head selection with prolong lifetime in wireless sensor network. J Soft Comput Eng Appl 2020;1(1):7.

[7] Rajesh P, Shajin FH, Cherukupalli K. An efficient hybrid tunicate swarm algorithm and radial basis function searching technique for maximum power point tracking in wind energy conversion system. J Eng Des Technol 2021.

[8] Shajin FH, Rajesh P, Raja MR. An efficient VLSI architecture for fast motion estimation exploiting zero motion prejudgment technique and a new quadrant-based search algorithm in HEVC. Circuit Syst Signal Process 2022;41(3):1751–1774.

[9] Liu SC, Lin SF. Robust sliding control for mismatched uncertain fuzzy time-delay systems using linear matrix inequality approach. J Chin Inst Eng 2013;36(5):589–597.

[10] Junyi C, Binggang C. Fractional-order control of pneumatic position servosystems. Math Probl Eng 2011;2011.

[11] Arunshankar J. Control of nonlinear two-tank hybrid system using sliding mode controller with fractional-order PI-D sliding surface. Comput Electr Eng 2018;71:953–965.

[12] Fellani MA, Gabaj AM. PID controller design for two tanks liquid level control system using Matlab. Int J Electr Comput Eng 2015;5(3):436.

[13] Demetriou MA. Spatial PID consensus controllers for distributed filters of distributed parameter systems. Syst Control Lett 2014;63:57–62.

[14] Carnevale C, Piazzi A, Visioli A. A methodology for integrated system identification, PID controller tuning and noncausal feedforward control design. IFAC Proc Vol 2008;41(2):13324–13329.

[15] Ram AG, Lincoln SA. Real time implementation of fuzzy based adaptive PI controller for a spherical tank system. Int J Simul Syst Sci Technol 2013;14:1–8.

[16] Chandra IS, Gajpal T. Fuzzy logic controller based impedance source converter for PV grid connected system. 2016;5(8):149–154.

[17] Abadi MR, Jalali AA. Fractional order PID controller tuning based on IMC. Int J Inf Technol Control Autom 2012;2:21–35.

[18] Ram SS, Kumar DD, Meenakshipriya B. Designing of PID controllers for pH neutralization process. Indian J Sci Technol 2016;9(12).

[19] Pandian BJ, Noel MM. Control of a bioreactor using a new partially supervised reinforcement learning algorithm. J Process Control 2018;69:16–29.

[20] Gurjar B, Chaudhari V, Kurode S. Parameter estimation based robust liquid level control of quadruple tank system–second order sliding mode approach. J Process Control 2021;104:1–10.

[21] Aksu IO, Coban R. Sliding mode PI control with backstepping approach for MIMO nonlinear cross-coupled tank systems. Int J Robust Nonlinear Control 2019;29(6):1854–1871.

[22] Meng X, Yu H, Zhang J, Xu T, Wu H, Yan K. Disturbance observer-based feedback linearization control for a quadruple-tank liquid level system. ISA Trans 2021.

[23] Bai T, Li S, Zou Y. Distributed MPC for reconfigurable architecture systems via alternating direction method of multipliers. IEEE/CAA J Autom Sin 2021;8(7):1336–1344.

[24] Song SJ, Cai G, Liao BL, Lin XF. Real-time optimal control for three-tank level system via improved ADDHP method. In: 2009 IEEE International Conference on Control and Automation. 2009.

[25] Hou Z, Liu S, Tian T. Lazy-learning-based data-driven model-free adaptive predictive control for a class of discrete-time nonlinear systems. IEEE Trans Neural Netw Learn Syst 2017;28(8):1914–1928.

[26] Radac MB, Precup RE, Roman RC. Data-driven model reference control of MIMO vertical tank systems with model-free VRFT and Q-learning. ISA Trans 2018;73:227–238.

[27] Khan MK, Spurgeon SK. Robust MIMO water level control in interconnected twin-tanks using second order sliding mode control. Control Eng Pract 2006;14(4):375–386.

[28] Pan H, Wong H, Kapila V, de Queiroz MS. Experimental validation of a nonlinear backstepping liquid level controller for a state coupled two tank system. Control Eng Pract 2005;13(1):27–40.

[29] Almutair NB, Zribi M. Sliding mode control of coupled tanks. Mechatronics 2006;16(7):427–441.

[30] Ng KC, Li Y, Murray-Smith DJ, Sharman KC. Genetic algorithms applied to fuzzy sliding mode controller design. In: First International Conference on Genetic Algorithms in Engineering Systems. 1995.

[31] Moshiri B, Jalili-Kharaajoo M, Besharati F. Application of fuzzy sliding mode based on genetic algorithms to control of robotic manipulators. Emerg Technol Factory Autom 2003;2:169–172.

[32] Benayache R, Chrifi-Alaoui L, Bussy P, Castelain JM. Design and implementation of sliding mode controller with varying boundary layer for a coupled tanks system. In: 17th Mediterranean Conference on Control & Automation. 2009. p. 1215–1220.

[33] Levant A. Chattering analysis. IEEE Trans Autom Control 2010;55(6):1380–1389.

[34] Floquet T, Spurgeon SK, Edwards C. An output feedback sliding mode control strategy for MIMO systems of arbitrary relative degree. Int J Robust Nonlinear Control 2010;21(2).

[35] Derdiyok A, Basci A. The application of chattering-free sliding mode controller in coupled tank liquid-level control system. Korean J Chem Eng 2013;30(3):540–545.

[36] Hou T. Experimental research on neural network PID control based on hydraulic pressure of 2 container water tank. J Lanzhou Jiaotong Univ 2009;28(3):41–43.

[37] Evans JT, Gomm JB, Williams D, Lisboa PJG. Implementation and performance evaluation of an on-line neural network control scheme. In: International Conference on Control. 1994.

[38] Ramli MS, Raja Ismail RMT, Ahmad MA, Mohamad Nawi S, Mat Hussin MA. Improved coupled tank liquid levels system based on swarm adaptive tuning of hybrid proportional-integral neural network controller. Am J Eng Appl Sci 2009;2.

[39] Zhang TP, Ge SS. Adaptive neural control of MIMO nonlinear state time-varying delay systems with unknown dead-zones and gain signs. Automatica 2007;43:1021–1033.

[40] Huang SJ, Chiou KC. An adaptive neural sliding mode controller for MIMO systems. J Intell Robot Syst 2006;46:285–301.

[41] Tan KC, Li Y. Performance-based control system design automation via evolutionary computing. Eng Appl Artif Intell 2001;14(4):473–486.

[42] Krohling RA, Rey JP. Design of optimal disturbance rejection PID controllers using genetic algorithm. IEEE Trans 2001;5:78–82.

[43] Fang XL, Shen T, Feng XS. The bang-bang control of water tank system based on fuzzy decision. In: Ninth International Conference on Hybrid Intelligent Systems. IEEE Press; 2009. p. 127–131.

[44] Khoei A, Hadidi Kh, Khorasani MR, Amirkhanzadeh R. Fuzzy level control of a tank with optimum valve movement. Fuzzy Sets Syst 2005;150:507–523.

[45] Yu J, Zhang T. Direct adaptive fuzzy control of nonlinear time-delay systems. Fuzzy Syst Math 2006;20(3):124–129.

[46] Li Q, Fang Y, Song J, Wang J. The application of fuzzy control in liquid level system. Measur Technol Mech Autom 2010;3:776–778.

[47] Basci A, Derdiyok A. Real-time velocity and direction angle control of an automated guided vehicle. Int J Robot Autom 2014;29(3):227–233.

[48] Wang L, Mishra J, Zhu Y, Yu X. An improved sliding-mode current control of induction machine in presence of voltage constraints. IEEE Trans Ind Inform 2020;16(2):1182–1191.

[49] Wang Z, Zhu YZ, Xue H, Liang HJ. Neural networks-based adaptive event-triggered consensus control for a class of multi-agent systems with communication faults. Neurocomputing 2022;470:99–108.

[50] Zhao X, Shi P, Zheng X, Zhang J. Intelligent tracking control for a class of uncertain high-order nonlinear systems. IEEE Trans Neural Netw Learn Syst 2019;21(9):1976–1982.

[51] He W, Dong Y, Sun C. Adaptive neural impedance control of a robotic manipulator with input saturation. IEEE Trans Syst Man Cybern 2016;46(3):334–344.

[52] Ngo TQ, Duong MK, Pham DC, Nguyen DN. Adaptive Wavelet CMAC tracking control for induction servomotor drive system. J Electr Eng Technol 2019;14(1):209–218.

[53] Yang R, Yang C, Chen M, Annamalai AS. Discrete-time optimal adaptive RBFNN control for robot manipulators with uncertain dynamics. Neurocomputing 2017;234:107–114.

[54] Wang Z, Yuan J, Pan Y, Wei J. Neural network-based adaptive fault tolerant consensus control for a class of high order multi-agent systems with input quantization and time-varying parameters. Neurocomputing 2017;266:315–324.

[55] Ngo TQ, Tran TH, Uyen HTT, Nguyen VT, Duong TD. Adaptive task-space control of five-bar parallel robot dynamic model with fully unknown using radial basis function neural networks for high-precision applications. J Robot Control 2025;6(4):1624–1635.

[56] Pham Q, Nguyen T, Tran T, Quynh B, Ngo T, Nguyen V, Le T. Raspberry Pi-based rapid control prototyping for PMSM drive system using RBFNN on OPAL-RT platform. Int J Robot Control Syst 2025;5(6):2669–2684.

Journal's webpage: http://univagora.ro/jour/index.php/ijccc/

This journal is a member of, and subscribes to the principles of,
the Committee on Publication Ethics (COPE).
https://publicationethics.org/members/international-journal-computers-communications-and-control

Cite this paper as:

Trung Nhan Nguyen; Thanh Quyen Ngo; Thanh Hai Tran; Ngoc Hoi Le; Van Sy Nguyen; Tong Tan Hoa Le (2026). Real-Time Hardware-in-the-Loop Evaluation of an RBFNN Controller for Water Level Control in an Uncertain Triple-Tank System, *International Journal of Computers Communications & Control*, 21(4), 7460, 2026.

https://doi.org/10.15837/ijccc.2026.4.7460